Effects of Solvent on the Formation of Octanethiol Self-Assembled Monolayers on Au(111) at High Temperatures in a Closed Vessel: A Scanning Tunneling Microscopy and X-ray Photoelec...

ARTICLE *in* THE JOURNAL OF PHYSICAL CHEMISTRY C · NOVEMBER 2012

Impact Factor: 4.77 · DOI: 10.1021/jp307940g

3 AUTHORS, INCLUDING:

Abdulla Hel Al Mamun
Chonbuk National University
10 PUBLICATIONS **31** CITATIONS

SEE PROFILE

THE JOURNAL OF PHYSICAL CHEMISTRY C

Article

pubs.acs.org/JPCC

Effects of Solvent on the Formation of Octanethiol Self-Assembled Monolayers on Au(111) at High Temperatures in a Closed Vessel: A Scanning Tunneling Microscopy and X-ray Photoelectron Spectroscopy Study

Abdulla Hel Al Mamun and Jae Ryang Hahn*

Department of Chemistry and Research Institute of Physics and Chemistry, Chonbuk National University, Jeonju 561-756, Korea

ABSTRACT: Self-assembled monolayers of 1-octanethiol (OT-SAMs) on Au(111) substrates prepared using ethanol, *N*,*N*′-dimethylformamide (DMF), toluene, or hexane were examined using scanning tunneling microscopy (STM) and X-ray photoelectron spectroscopy (XPS) to investigate the effects of the solvent on the molecular packing at high solution temperatures (90 °C) and high pressures (21 psi) in a closed vessel. STM imaging revealed the formation of ordered OT-SAMs with a $(3 \times \sqrt{7})$R11° overlayer structure on Au(111) surfaces in ethanol, whereas OT-SAMs prepared in DMF revealed large ordered domains with a $(\sqrt{3} \times \sqrt{3})$R30° phase and a $c(4 \times 2)$ superstructure. OT-SAMs prepared in toluene produced a mixture of ordered and striped phases, while no clear ordered structures were observed for OT-SAMs prepared in hexane. The disposition of OT bound to the Au(111) surfaces depended on the solvent, which also affected whether the OT-SAMs formed ordered or disordered phases. The intensities of XPS peaks at 161 and 162.3 eV increased with domain disorder, possibly due to changes in the adsorption configurations of the OT molecules.

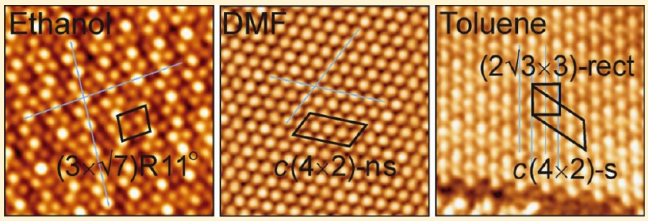

1. INTRODUCTION

Organic thiols form self-assembled monolayers (SAMs) on metallic surfaces and provide an excellent means for controlling surface properties at the molecular level.[1−7] The self-assembly process relies on mutual specific recognition of fundamental building blocks and the spontaneous formation of well-organized structures without human intervention.[8] A widely studied class of SAMs includes alkanethiol monolayers supported on metal substrates, such as the (111) surface of gold. SAMs on Au(111) are easily prepared, yield high-quality two-dimensional ordered structures, and are versatile with respect to the tunability of chemical functional groups. The formation of alkanethiol-SAMs from solution involves rapid initial physisorption onto the gold substrate followed by slow chemisorption and loss of a proton.[9] Thiol molecules are strongly bound to the Au(111) surface through the sulfur headgroup, and their alkyl chains are directed away from the metal surface.[10,11] The growth of high-density domains is accompanied by formation of gold vacancy islands that nucleate outside of the ordered domains.[12−14]

Molecular-scale images reveal that alkanethiol SAMs commonly form a $(\sqrt{3} \times \sqrt{3})$R30° structure on Au(111) surfaces, and $c(4 \times 2)$ superlattices (also referred to as $c(4\sqrt{3} \times 2\sqrt{3})$R30° or $2\sqrt{3} \times 3$ in the literature) may also be present,[15] depending on the thiol chain length[16] and the presence of surface defects.[17,18] The $c(4 \times 2)$ and $(\sqrt{3} \times \sqrt{3})$R30° phases may be standing-up phases in which the alkyl chains are tilted from the surface normal by ∼30°. Since its first discovery,[19] at least five different forms of $c(4 \times 2)$ structure have been reported, each with the same $c(4 \times 2)$ lattice frame, but with subtle differences in the nature of the unit cell.[20,21] Although various structural models have been proposed to account for these different $c(4 \times 2)$ structures, the connection between structures and indeed a relationship between the $c(4 \times 2)$ and $(\sqrt{3} \times \sqrt{3})$R30° phases remain far from apparent. The $c(4 \times 2)$ structures can be classified into two groups depending on whether the adsorbate position exhibits a noticeable lateral shift ($c(4 \times 2)$-s, shifted) or not ($c(4 \times 2)$-ns, nonshifted) from those in the $(\sqrt{3} \times \sqrt{3})$R30° phase. The $c(4 \times 2)$-s denotes a structure in which neighboring adsorbates shift laterally toward each other, although the positional shift involves a mobile adsorbate moving toward a stationary adsorbate within the same domain. The $c(4 \times 2)$-ns showed modulated brightness contrasts within the $c(4 \times 2)$ unit cell in STM images, but no significant shift in lateral position was observed in the $(\sqrt{3} \times \sqrt{3})$R30° structure.[20−26]

Considerable effort has been devoted to the preparation of defect-free films or the modification of film structures by controlling, for example, substrate morphology, alkanethiol purity, and deposition parameters including solvent, deposition time, alkanethiol concentration, temperature, and pressure.[7,8,27−30] Among the variety of solvents used, ethanol, *N*,*N*′-dimethylformamide (DMF), toluene, hexadecane, and cyclooctane did not affect the thickness of hexadecanethiol

Received: August 9, 2012
Revised: September 26, 2012
Published: October 5, 2012

   dx.doi.org/10.1021/jp307940g | *J. Phys. Chem. C* 2012, 116, 22441−22448

SAMs;[30] however, SAM formation kinetics in certain nonpolar solvents exceeded those observed in polar protic solvents.[31,32] Scanning tunneling microscopy (STM) images of OT-SAMs have shown that $c(4 \times 2)$ phases form in ethanol, whereas $5 \times \sqrt{3}$ striped phases form in toluene on Au(111) surfaces at 50 °C.[33] Although the solution temperature during immersion may be crucial for determining the final SAM structure,[7,29,34] the solvent itself is another important factor for controlling the SAM surface structure.[35−38] The size of well-ordered domains and the number of depressions in alkanethiol-SAMs on gold may be strongly influenced by the solvent and immersion temperature.[33,36] Therefore, an appropriate solvent must be selected to obtain SAMs suitable for a desired purpose.[39,40]

Thermal processing may induce lateral movement of molecules on the metal surface and influence the formation of ordered domains and boundaries. Dry annealing of SAMs can increase the coherence length of a SAM to >100 nm, although concurrent thiolate desorption can generate defects within domains.[41] A SAM may be heated in the presence of a solution containing excess thiol to counteract this process. With this technique, structural domains may be quite large, limited only by the size of the terraces of the underlying substrate, which is important for applications in which chemical protection of a substrate or a highly uniform electronically insulating film is needed. Disorder in a monolayer can enhance exchange through greater access of the solution to the Au substrate and acceleration of alkanethiolate desorption. Solvation of the thiolate and thiolate−Au species may also be involved. Higher temperatures increase the surface diffusion of both the alkanethiolate and the Au substrate.[42−46] Heating in a thiol solution facilitates Ostwald ripening of SAM domains by desorption, adsorption, and diffusion.[47] Higher immersion temperature at elevated pressures in ethanol solvent can induce a structural transition of SAM as well as the larger domains with a lower density of vacancy.[29] An oblique $(\sqrt{3} \times \sqrt{3})R30°$ OT-SAM structure was observed below the normal boiling point, whereas a superstructure $(3 \times \sqrt{7})R11°$ covered the gold surfaces at 90 °C.

In this study, we investigated the effect of solvent on the formation of OT-SAMs on Au(111) surfaces at 90 °C at an elevated pressure (21 psi). A higher temperature and pressure were chosen to minimize the defect density and to maximize the domain size to achieve a high packing density. It also facilitates the formation of SAM and overcome a possible unknown kinetic barrier. The molecular-scale structures and binding characteristics of OT-SAMs were characterized using STM and X-ray photoelectron spectroscopy (XPS). Four solvents with distinct dipole moments and other properties were tested: ethanol (polar protic with 1.69 D), DMF (polar aprotic with 3.86 D), toluene (0.36 D), and hexane (nonpolar). The domain structures and molecular configurations of OT-SAMs depended on the solvent type, and the degree of disorder in OT-SAM films could be measured from the relative intensity of XPS peaks, which were sensitive to changes in the adsorption configuration.

2. EXPERIMENTAL SECTION

1-Octanethiol ($CH_3(CH_2)_7SH$, ≥98.5% purity, Aldrich) was used without further purification. Ethanol (Aldrich), DMF (Aldrich), toluene (Aldrich), and hexane (Aldrich) were used as received (≥99%). Au(111) surfaces were prepared by vapor deposition of gold onto freshly cleaved heated muscovite mica or onto a bead formed at the end of a Au wire. All gold substrates were hydrogen flame annealed immediately before use. OT-SAMs were formed by immersing the Au(111) substrate into a solution containing OT (1 mM) in a stainless steel bath sealed by the bolted copper gaskets at 90 °C for 24 h, conditions that yielded pressures ~21 ± 0.5 psi. Samples were then allowed to cool to room temperature, rinsed with the respective solvent to remove weakly adsorbed species (dipping method), and dried under a flow of nitrogen. This method differs from vacuum annealing[11] and air annealing[48] as the sample was continuously exposed to alkanethiol vapor and vapor-annealing[49] methods for postpreparative modification of SAMs. We found that our approach produced very high quality OT-SAMs, but initial attempts to use longer chain alkanethiols were not as successful. All STM images reported here were obtained by STM (SOLVER P47, NT-MDT) under ambient conditions. The tips were prepared by mechanically cutting from a 0.20 mm diameter platinum/iridium wire. The data were collected in the constant current mode using tunneling currents between 40 and 150 pA and sample bias voltages between 100 and 600 mV. These imaging conditions did not affect SAM structures to produce structural defects or transitions during STM imaging. High-resolution XPS spectra were obtained using an AXIS-NOVA X-ray photoelectron spectrometer (Kratos Inc. Manchester, UK) with a monochromatic Al Kα (1486.6 eV) X-ray source at an 8.0×10^{-9} Torr base pressure. Binding energy (BE) scales for the monolayers on gold were referenced by setting the BE of $Au_{4f_{7/2}}$ to 84.0 eV. High-resolution S 2p spectra were acquired with an analyzer pass energy of 50 eV. All XPS data were acquired at a nominal photoelectron takeoff angle of 45°, where the takeoff angle was defined as the angle between the surface normal and the axis of the analyzer lens.

3. RESULTS AND DISCUSSION

Figure 1 shows STM topographical images of OT-SAMs on Au(111) surfaces modified in ethanol (a), DMF (b), toluene (c), or hexane (d) solutions containing 1 mM OT at 90 °C for 24 h in a sealed bath. The STM image of the OT-SAM formed in ethanol (Figure 1a) shows features typical of a gold surface covered with an alkanethiol SAM, including pits and domain boundaries. The average pit depth was 2.4 Å, which was approximately equal to the monatomic step height of the Au(111) surface. These pits were assigned to vacancy islands on the gold surface. The number of pits per 200 × 200 nm^2 area on the SAMs was 90 ± 2, and the average sizes of the ordered domains and pits were 25 ± 2 and 14 ± 2.0 nm, respectively. A comparison of SAMs prepared at 90 °C and room temperature[50−52] revealed an increase in the average pit size and a corresponding decrease in the pit density with the higher preparation temperature. It should be noted that the pits were not free of OT molecules; rather, they were fully coated with OT-SAM. A consequence of the reduced pit density and pit size was that SAMs were almost defect-free. Interestingly, the grain boundary, which was often found with SAMs prepared at room temperature in ethanol solvent, was not observed in our work.

SAMs prepared in DMF (Figure 1b) included pits that tended to be connected, and the densities of the steps and defects were very low, resulting in larger domains. In this case, the number of pits was 22 ± 2, and the average sizes of the ordered domains and pits were >40 and 18 ± 4 nm, respectively. The formation of low-density vacancy islands

dx.doi.org/10.1021/jp307940g | J. Phys. Chem. C 2012, 116, 22441−22448

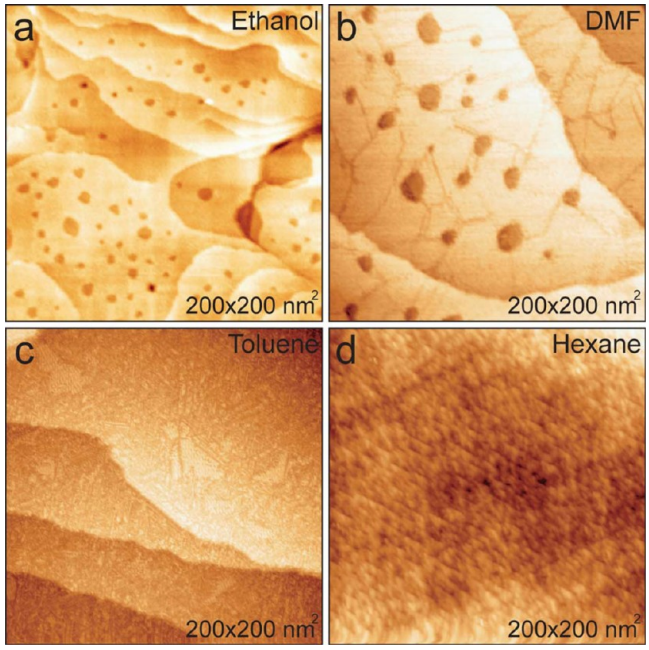

Figure 1. STM topographical images of Au(111) surfaces (bead) covered with OT-SAMs formed by immersion for 24 h in 1 mM OT (a) ethanol, (b) DMF, (c) toluene, or (d) hexane solution at 90 °C in a sealed stainless steel bath. The sample bias voltages and tunneling currents were 250 mV and 55 pA for (a), 150 mV and 60 pA for (b), 200 mV and 50 pA for (c), and 180 mV and 40 pA for (d), respectively. The scan areas were 200 × 200 nm^2 for all images.

seems to be related to alkanethiol mobility changes in different solvents. Au adatoms and vacancy islands diffused rapidly on the surface and merged near the step edges because of a reduction in the total step edge energy, which resulted in the formation of low-density vacancy islands.[2,53] A higher rate of diffusion for OT in DMF may have resulted in the formation of a large, single domain, as shown in Figure 1b. The pits were connected by shallower depression grooves. This domain structure resembled that of a 1-decanethiol SAM formed in ethanol followed by annealing for 1 h in air.[48] The formation of grooves resulted from lower alkanethiol coverage, which prevented the molecules from orienting orthogonal to the metal surface. Increasing the annealing time to 2 h led to partial desorption of the alkanethiol monolayer. The use of solvents that enable thiolates to crystallize into large domains of a $(\sqrt{3} \times \sqrt{3})$R30° lattice can result in enhanced chain densities and fewer defects within the SAM. Less polar solvents interact weakly with the adsorbates and provide less perturbation of interchain interactions of thiolates during assembly, while more polar solvents may facilitate crystallization into larger domains.[54] In contrast to the formation of OT-SAMs in ethanol or DMF, OT-SAMs prepared in toluene mainly exhibited disordered phases containing relatively small areas of ordered phases, as shown in Figure 1c. Steps and molecular terraces were readily apparent, although it was very difficult to identify the regular shape of pits. The structure of the OT-SAM prepared in hexane differed significantly from the structures of the other OT-SAMs (Figure 1d). No clear step features were observed, although flat regions could be resolved. Pits were present with no clear boundaries, and a magnified STM image revealed the lack of an ordered structure.

The solvent also affected the molecular configuration of OT-SAMs on the Au(111) surface. A high-resolution STM image (shown in Figure 2a and see below) of an OT-SAM formed in ethanol revealed the presence of a $(3 \times \sqrt{7})$R11° super-

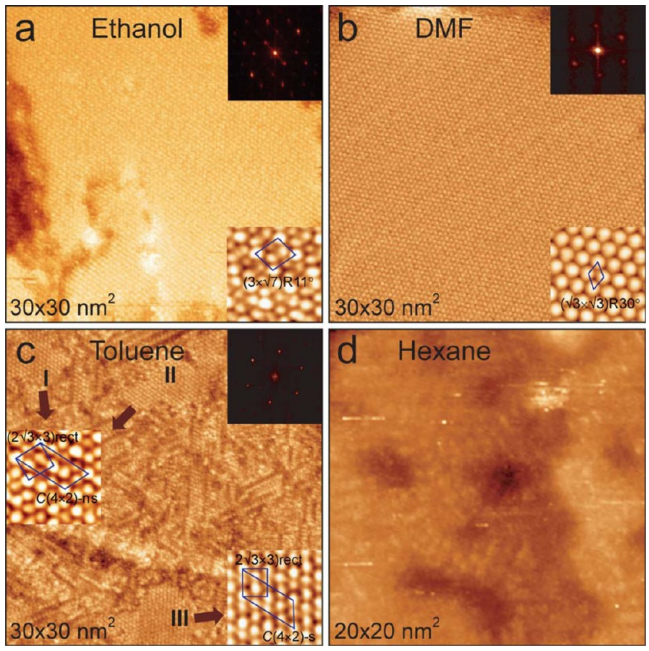

Figure 2. STM topographical images of Au(111) surfaces (bead) modified in 1 mM OT (a) ethanol, (b) DMF, (c) toluene, or (d) hexane solution after incubation at 90 °C for 24 h in a sealed stainless steel bath. The insets in (a), (b), and (c) show 2-D fast Fourier transforms and high-resolution images. The inset (down) in (b) indicates the presence of a $c(4 \times 2)$-ns structure in which no relative positional shift occurred. On the other hand, the inset (down) in (c) indicated a $c(4 \times 2)$-s structure characterized by a lateral positional shift of OT molecules. The sample bias voltages and tunneling currents were 550 mV and 130 pA for (a), 600 mV and 150 pA for (b), 560 mV and 140 pA for (c), and 550 mV and 130 pA for (d). The scan areas are indicated in each image.

structure, which differed from the $(\sqrt{3} \times \sqrt{3})$R30° overlayer structure formed below 75 °C in ethanol. In DMF, closely packed and well-ordered OT-SAMs with long-range ordered structures were observed. The observed periodic arrangement of protrusions that assumed a hexagonal $(\sqrt{3} \times \sqrt{3})$R30° structure may have formed due to occupation of equivalent 3-fold hollow sites of the Au(111) lattice.[55] The average spacing between alkyl chains (protrusions) was 5 Å. The chain spacing corresponded closely to the 4.99 Å distance between neighboring sulfur atoms. The adsorption of OT in toluene produced many defects as well as ordered and striped phases. The average size of ordered domains was ~8 nm. The striped phase had a lower packing density, in which the molecular backbone was oriented parallel to the Au(111) substrate (Figure 2c). Three domains are labeled in Figure 2c. At the upper part of the image, domains I and II have the same structures as shown in the inset. Domain III has a different configuration from domains I and II. For domains I and II, a nonshifted $c(4 \times 2)$ structure was found while a noticeable lateral shift ($c(4 \times 2)$-s structure) was observed for domain III. Such striped phases have been observed either during growth or after annealing in a vacuum.[56−61] In general, the spacing between stripes is comparable to twice the alkyl chain length. Thus, stripe formation by alkanethiol molecules has been thought to result from a configuration in which the alkane

dx.doi.org/10.1021/jp307940g | J. Phys. Chem. C 2012, 116, 22441−22448

chains lay nearly flat on the surfaces at both sides of the stripe. This configuration was particularly true for vacuum-annealed samples, as studied by He atom scattering[41,57] and STM.[61]

In contrast to the other SAM samples with ordered structures, OT molecules in hexane led only to formation of disordered phases, as shown in Figure 2d. Toluene and hexane can be classified as nonpolar solvents; however, the formation and final structures of SAMs differed significantly in these solvents. We suggest that the interactions between hexane and OT are stronger than those between toluene and OT because hexane and OT share an alkyl backbone structure. These strong interactions may reduce lateral interactions among OT molecules in the SAM by incorporating solvent molecules into the monolayers, thereby forming a disordered phase.[8,30] A full description of solvent effects is difficult because solvent properties, including polarity, solubility, molecular diameter, and viscosity, can affect solvent−gold substrate and solvent−adsorbate interactions during SAM formation.[62]

The domains formed in ethanol, DMF, and toluene were analyzed via high-resolution STM image of OT-SAMs with cross-sectional cuts, as shown in Figures 3 and 4. Figure 3a shows a high-resolution STM image of an ordered domain formed in ethanol, which revealed the presence of a structural phase not seen for samples prepared in the other solvents. Figure 3c shows a height profile along the nearest-neighbor direction in the STM image (line A in Figure 3a). The distance between pairs of bright protrusions was 8.7 ± 0.2 Å, three times the size of a Au atom ($3a_h$). The height profile along the next-nearest-neighbor direction in the STM image (not shown in Figure 3a) showed a periodicity of 7.6 ± 0.2 Å, which

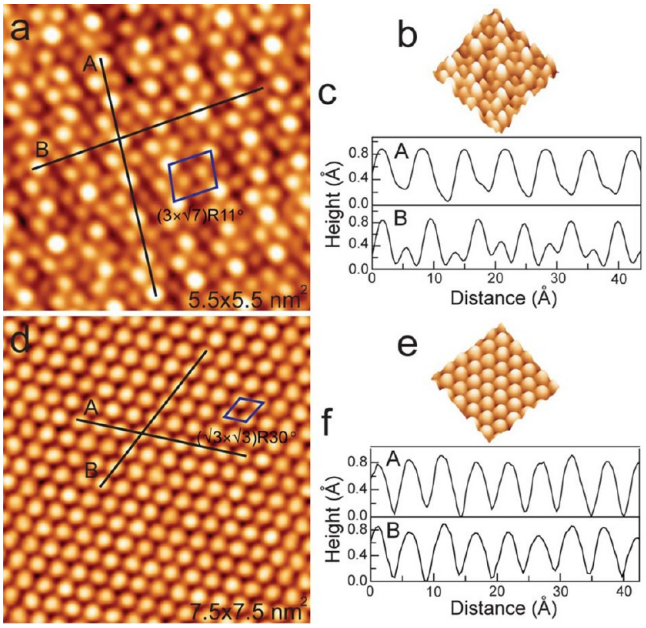

Figure 3. High-resolution STM topographical images were obtained from one ordered domain of the OT-SAM prepared by immersion in 1 mM OT (a) ethanol and (d) DMF solution after incubation at 90 °C for 24 h in a sealed stainless steel bath. These images were taken with a sample bias voltage of 600 mV and a tunneling current of 150 pA for (a) and 600 mV and 140 pA for (d), respectively. The scan area was 55 × 55 and 75 × 75 Å^2 for (a) and (d), respectively. Parts (c) and (f) show the cross-sectional height profiles of images (a) and (d), respectively. The corresponding three-dimensional images are shown in (b) and (e).

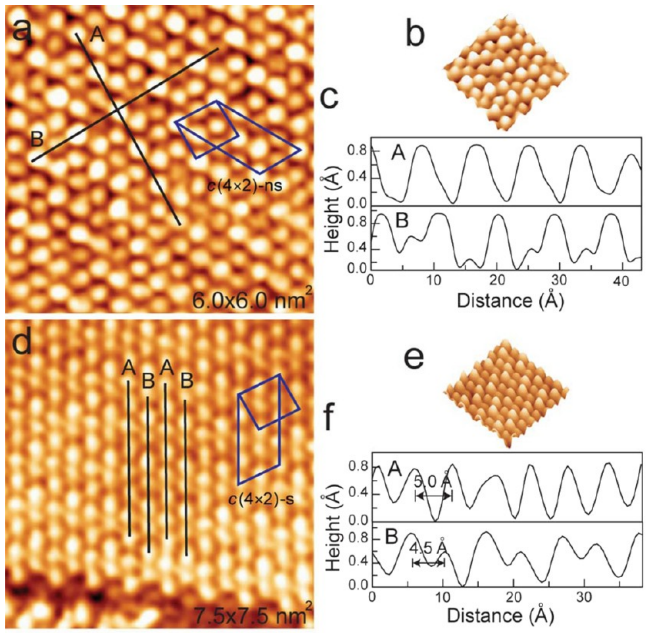

Figure 4. High-resolution STM topographical images were obtained from two types of ordered domain of the OT-SAM prepared by immersion in 1 mM OT toluene solution after incubation at 90 °C for 24 h in a sealed stainless steel bath. Image (a) was obtained from domain I or II and image (d) from domain III in Figure 2c. These images were taken with a sample bias voltage of 560 mV and a tunneling current of 140 pA. The scan area was 60 × 60 Å^2 and 75 × 75 Å^2 for (a) and (d), respectively. Parts (c) and (f) show the cross-sectional height profiles of iamges (a) and (d), respectively. The corresponding three-dimensional images are shown in (b) and (e).

corresponds to a distance of $\sqrt{7}a_h$. The molecularly resolved image, shown in the inset of Figure 2a, revealed an oblique unit mesh with cell dimensions of 8.7 × 7.6 Å^2 containing four OT molecules that form a (3 × $\sqrt{7}$)R11° superlattice. The (3 × $\sqrt{7}$)R11° superlattice revealed four distinguishable non-equivalent octanethiolates with different topographical heights per unit cell. A small difference in geometric height (~0.3 Å) was observed for the adsorption sites, and the adsorption energy on different sites was marginally different.[63] It is possible therefore that OT molecules adsorbed onto different types of sites such as the 3-fold hollow (fcc and hcp), on the top Au sites, or at the bridging sites of the Au(111) surface.[64]

A high-resolution STM image of the OT-SAM formed in DMF revealed close-packed ordered phases that formed a c(4 × 2) superlattice with respect to the Au(111) lattice (Figure 3d). A height profile across the close-packing direction on the STM image (Figure 3c) is shown in Figure 3f. The profile coincided with one of the three close-packing directions in the ($\sqrt{3}$ × $\sqrt{3}$)R30° phase, which indicated that the nearest-neighbor distance among the adsorbates was 5 Å or $\sqrt{3}a_h$. The inset image in Figure 2b reveals a c(4 × 2)-ns structure of OT-SAM domains. The average spacing between alkyl chains (protrusions) was 5 Å. This spacing was nearly 3 times that of the van der Waals diameter of a sulfur atom (1.85 Å), suggesting the presence of minimal S−S interactions.[65] This distance was also greater than the distance of closest approach of the alkyl chains (4.24 Å); therefore, the alkyl chains were tilted naturally at an angle of 30° with respect to the surface normal to maximize their van der Waals interactions as they packed into the final crystalline monolayer.[30,66] The hexagonal ($\sqrt{3}$ × $\sqrt{3}$)R30°

dx.doi.org/10.1021/jp307940g | J. Phys. Chem. C 2012, 116, 22441−22448

unit cell consisted of one molecule, and the area occupied by the single molecule was 21.6 Å^2.

Molecular scale images of the OT monolayer deposited from toluene revealed the generation of both a $c(4 \times 2)$-ns structure and ABAB ordered SAMs in a $c(4 \times 2)$-s superlattice configuration with respect to the Au(111) lattice (Figure 4). Cross-sectional cuts along lines A and B in Figure 4a (Figure 4c) revealed that the distance between two bright protrusions along the nearest-neighbor direction was 9.9 ± 0.2 Å or $2\sqrt{3}a_h$. The height profile line along the next-nearest-neighbor direction showed a periodicity of 8.6 ± 0.2 Å or $3a_h$. The unit cell of the $c(4 \times 2)$-ns superlattice is therefore orthorhombic, $(2\sqrt{3} \times 3)$-rect with a dimension of 9.9 × 8.6 Å^2. The unit cell was 4 times larger than the $(\sqrt{3} \times \sqrt{3})$R30° lattice and included four molecules.

The height profiles along lines A and B in Figure 4d (Figure 4f) showed significant lateral displacement among the adsorbate positions. The distance between adjacent bright spots along line A was 5 Å or $\sqrt{3}a_h$, and the distance between bright spots and the nearest dim spot along line B was 4.5 Å. Dim spots within the $c(4 \times 2)$ superlattice were shifted 0.05 ± 0.02 nm toward the bright spots, which is consistent with displacement of thiol molecules from hollow to bridge sites.[67] The two images of Figure 4a,d may indicate a pathway for structural transformation from $(\sqrt{3} \times \sqrt{3})$R30° to $c(4 \times 2)$-ns and then to $c(4 \times 2)$-s. The $c(4 \times 2)$-ns structure could be an intermediate between the $(\sqrt{3} \times \sqrt{3})$R30° and $c(4 \times 2)$-s structures.

Positional shifts of the adsorbates can give rise to the structural transformation from $(\sqrt{3} \times \sqrt{3})$R30° to $c(4 \times 2)$-s. The reason for the contrast between bright and less bright spots in the $c(4 \times 2)$-s phase remains unclear. The $c(4 \times 2)$-s phase may actually be close to a $c(4 \times 2)$-ns phase. For example, a shift in the adsorbate position from a hollow site may be too small for detection using STM, which would instead detect the presence of an apparent $c(4 \times 2)$-ns structure. Au(111) surfaces are slightly rippled such that gold surface atoms are easily compressed on a clean surface. The gold atoms can shift laterally along the close-packing direction to form a well-known herringbone reconstruction on a clean surface. The addition of atoms or molecules to the surface can modify this surface reconstruction. The full $(\sqrt{3} \times \sqrt{3})$R30° phase of alkanethiol self-assembled monolayers appears to have completely lifted the substrate reconstruction. The atoms on the underlying Au(111) surface can shift upward in a regular manner while maintaining a $(\sqrt{3} \times \sqrt{3})$R30° geometry.

On the basis of the STM images, we propose a schematic model to explain the $(3 \times \sqrt{7})$R11° superlattice and two types of $c(4 \times 2)$ structure, as shown in Figure 5. The STM images of an OT-SAM formed in ethanol show that the molecular arrangements of the phases clearly deviate from the hexagonal packing previously observed with saturated alkanethiol SAM coverage. In this model (Figure 5a), the unit cell consists of four inequivalent molecules with an area of 16.4 Å^2 per molecule, which is denser than that of the hexagonal $(\sqrt{3} \times \sqrt{3})$R30° unit cell (21.6 Å^2 per molecule). The sulfur atoms are bound to several adsorption sites, such as the 3-fold hollow, top, or bridging sites. Displacement of pinning sites for sulfur atoms from the hollow to top site is ~0.6 Å and from the hollow to bridge site is ~0.5 Å, which is consistent with previously reported results.[64,67] The height difference between adsorption sites is ~0.3 Å, and the adsorption energies of the sites are comparable.[68] The van der Waals interactions between

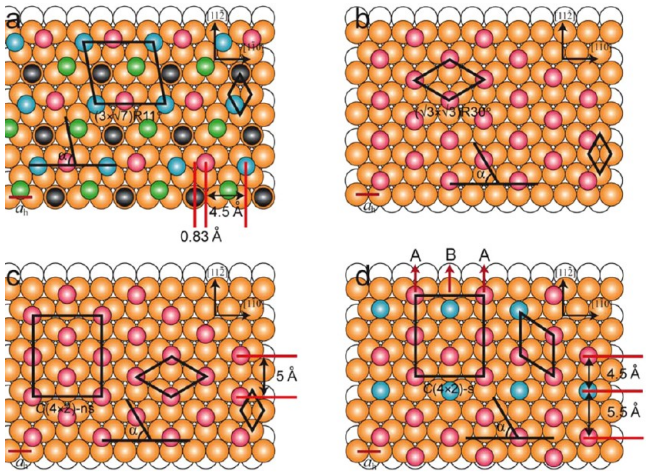

Figure 5. (a) A schematic model describing the configuration of the proposed $(3 \times \sqrt{7})$R11° superlattice based on STM images. The oblique unit mesh consisted of four OT molecules, and the lattice constants of the unit cell were a = 8.7 Å, b = 7.6 Å, and α = 79°, and a_h = 2.89 Å, which denotes the atomic spacing of the Au(111) lattice. (b) The structural model of the $(\sqrt{3} \times \sqrt{3})$R30° superlattice. (c) and (d) show schematic models of the two $c(4 \times 2)$ structures. In the case of (c), the structure represents the $c(4 \times 2)$-ns phase, with adsorbates at the same lattice sites as those in the $(\sqrt{3} \times \sqrt{3})$R30° structure. (d) shows a $c(4 \times 2)$-s structure in which every other molecule is shifted up to the nearest bridging site along line B. The gold-colored and empty circles represent Au atoms in the top and second layers, respectively. Other circles represent S atoms adsorbed near the 3-fold hollow (fcc and hcp), on top Au sites, or at bridging sites of the Au(111) surface. Circles are scaled according to the covalent radii of Au and S atoms.

molecular chains is important to the overall organization of the adsorbates. We therefore conclude that the phase transitions mainly arise from migration of octanethiolate groups from the 3-fold hollow to bridge or top Au sites in alternating rows along the nearest-neighbor direction.

Figure 5b shows the structure of an OT-SAM in which sulfur atoms were bound to 3-fold sites in the $(\sqrt{3} \times \sqrt{3})$R30° phase, which further arranged in a $c(4 \times 2)$-ns superstructure, as shown in Figure 5c. The sulfur binding sites have yet to be successfully characterized. Early studies suggested that the sulfur heads were pinned to the 3-fold hollow sites of the surface.[1,69] Later, Fenter et al.[64,68] proposed a model which remains under debate, in which S−S groups were paired with alternating bridge/hollow sites to achieve sulfur−gold bonding and the chains assumed conformations with gauche S−C bonds that arranged the methyl groups in hexagonal symmetry at the outer surfaces. The observed S−S pairing feature may have resulted from interfacial structural damage due to X-ray secondary electron generation[70] or annealing.[71] The model described here assumes that the thiol groups were bonded to the most stable Au(111) sites in the $(\sqrt{3} \times \sqrt{3})$R30° structure. Controversial theoretical studies of these sites—the top,[72] bridge,[73] hollow,[74] or sites between the hollow and bridge[75]—led us to select the most common feature for Au−S bonding in our model, i.e., the 3-fold hollow site and any observed deviations from it.

Figure 5d shows a $c(4 \times 2)$-s structure in which one OT in the unit cell was shifted to a bridge site; however, the shift was less extensive than that observed in the $(3 \times \sqrt{7})$R11° structure (Figure 5a). The adsorption energies of the 3-fold

dx.doi.org/10.1021/jp307940g | J. Phys. Chem. C 2012, 116, 22441−22448

hollow and bridge sites were expected to differ; however, the energy difference may be minimized by adjusting the distance between alkane chains. This model is one of several suggested previously,[72] in which the distance between bright and less-bright neighboring spots along line B was 4.5 Å. The ball models in Figure 5 suggest that different $c(4 \times 2)$ structures may be obtained, depending on the degree of the adsorbate shift in the $[11\bar{2}]$ direction. In fact, previous STM studies[20,21,25,65,76] have identified more than two characteristic distances between pairs of monothiolates, in agreement with our model. It is possible that the adsorbates do not occupy high-symmetry sites due to alkane chain steric effects. As two thiolates move closer together, the alkane chains can adjust their conformation, such as tilt angle, to compensate for energy increases due to the adsorbate moving onto a low-symmetry site.

To investigate the effects of solvent on the binding characteristics of the OT sulfur headgroup on the gold surface, we examined XPS spectra in the S 2p region of OT-SAM samples prepared in the four solvent systems: ethanol, DMF, toluene, or hexane. Figure 6 displays the large differences in the

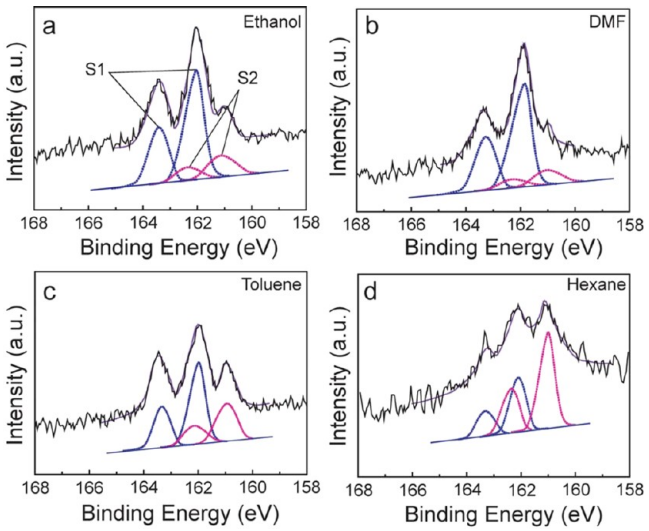

Figure 6. A series of XPS spectra in the S(2p) region of OT-SAMs on Au(111) surfaces on mica obtained in (a) ethanol, (b) DMF, (c) toluene, or (d) hexane solvent at 90 °C after immersion for 24 h in a sealed stainless steel bath. The upper (black line) and lower (blue and red lines) spectra correspond to the observed spectrum and resolved peaks, respectively. All of the peaks were resolved using a mixture of Gaussian and Lorentzian profiles with a peak ratio of 9:1.

S 2p spectra for the four SAM samples, indicating that solvent properties significantly affected the OT adsorption process during self-assembly. The S 2p peak usually appears as a doublet composed of $2p_{3/2}$ and $2p_{1/2}$ peaks with an intensity ratio of 2:1 that originates from spin−orbital splitting.[77−81] Figure 6 shows four peaks that are attributed to two different sulfur species. Stronger binding peaks (peak S1) were observed at 162.0 (S $2p_{3/2}$) and 163.3 eV (S $2p_{1/2}$), while weaker binding peaks (peak S2) were observed at 161.0 (S $2p_{3/2}$) and 162.3 eV (S $2p_{1/2}$). The peaks had a full width at half-maximum of 0.78. A chemisorbed sulfur peak (peak S1) is frequently observed in XPS spectra of well-ordered alkanethiol SAMs on gold. A peak induced by unbound sulfur above 163.5 eV[77] was not observed in the present work. Chemical bond formation between the sulfur and Au surface decreased the S(2p) binding energy, indicating that OT was chemisorbed on the gold surface. It should be noted that the S(2p) peak position did not depend strongly on the solvent species, as the solvent did not affect the S(2p) binding energy.

An additional chemisorbed peak (peak S2) differentiated the XPS spectra of the four OT-SAM samples and was associated with a distinct intensity for each sample. The intensity of the S2 peak was lowest for the OT-SAM prepared in DMF, slightly higher for the OT-SAM prepared in ethanol, much higher for the SAM prepared in toluene, and highest for the hexane-prepared SAM. Our STM and XPS observations suggested that the intensity of the S2 peak increased with increasing surface disorder (molecular randomness) and was closely related to the adsorption configuration of OT molecules. The S2 peak may arise from different sulfur binding geometries, which would change the adsorption configuration of OT molecules;[78,79,82,83] alternatively, this peak may arise from changes in the adsorption sites of the sulfur atoms on the Au(111) surface.[79,84] The S2 peak of alkanethiol and dialkyl disulfide SAMs has been observed after annealing in a vacuum at high temperatures, in low-coverage SAMs after annealing in air, and during the initial stages of SAM growth.[78] In the SAM prepared in DMF, the sulfur binding sites were equivalent, whereas other sites were available in ethanol and toluene. Large regions of disordered phases in SAMs prepared in toluene or hexane indicated the presence of different binding sites. Some of the sulfur atoms may have assumed a configuration with the alkyl chains nearly parallel to the surface in the disordered phase and interacted strongly with the gold surface. This configuration, which gave rise to the S2 peak, is consistent with the configuration observed in low-coverage alkanethiol-SAMs containing a striped phase in which the alkyl backbone was oriented parallel to the surface.[79] We conclude that OT binding conditions on the Au(111) surface largely depend on solvent properties, which determine whether OT-SAMs assume ordered or disordered phases.

Surface diffusion of alkanethiols plays important roles in the self-assembly process.[85,86] Thus, solvent was expected to affect the structure of SAMs. In addition, if the etching process of gold occurs in the process, the solvent polarity should affect the density and shape of vacancy islands on the gold surface. In most studies, ethanol solvent has been used in modifications, and while a solvent effect on microscopic features of SAMs has not been well studied, there have been several reports of solvent effects on macroscopic features.[86] The presence of a solvent adds additional parameters to the dynamic equilibrium governing the adsorption of thiols: solvent−substrate and solvent−adsorbate interactions as well as adsorbate−adsorbate interactions complicate the thermodynamics and kinetics of the assembly process. Solvent−substrate interactions can hinder the rate of adsorption of thiols from solution because solvent molecules must be displaced from the surface prior to adsorption of thiols, which are less prevalent in solution than solvating molecules. Elevated temperatures and pressures may increase the desorption rate of adventitious materials and solvent molecules physisorbed on the surface of the substrate and allow the system to more easily cross-activation barriers for processes such as chain reorganization and lateral rearrangements of the adsorbates.

Solvent polarity is defined as the overall solvation capability of a solvent, which in turn depends on the action of all possible nonspecific and specific intermolecular interactions between solute and solvent molecules. These interactions lead to definite

chemical alterations of the molecules of the solute. The solubility of OT in the solvents employed in the present work decreases in the order ethanol > DMF > toluene > hexane,[88,89] and the solubility of OT nearly always increases with temperature. Our STM results indicate that assembly solvents with high polarity can improve the quality of SAMs, while the quality of SAMs was poor with low polarity solvents in agreement with previous reports.[90−94] It is also possible that strong hydrophobic interactions between the nonpolar hydrocarbon tail of OT-SAMs and a solvent of low polarity loosens the tight packing of the monolayer. High-quality SAMs that possess more ordered structure can form in solvents with high solubility; solvent molecules with low solubility are not bound strongly to each other and are therefore free to interact with the alkyl chains of the thiol monolayer.[95,96]

4. CONCLUSIONS

We have demonstrated that solvent properties affect the domain structure, binding sites, packing density, and binding characteristics of OT-SAMs on Au(111) surfaces prepared at 90 °C in a sealed bath under high pressures. Ordered OT-SAMs were obtained using polar solvents, such as ethanol or DMF. High-resolution STM images revealed that OT-SAMs formed in ethanol on Au(111) had a $(3 \times \sqrt{7})$R11° overlayer structure. Variations in the topographical heights were attributed to the preference of the sulfur headgroup to bind to four adsorption sites on Au(111). OT-SAMs prepared in DMF yielded a hexagonal $(\sqrt{3} \times \sqrt{3})$R30° structure, with connected vacancy islands and a very low defect density resulting in larger domains. On the other hand, toluene induced formation of both ordered and striped phases for the OT-SAM, with ordered phases exhibiting both $c(4 \times 2)$-ns and $c(4 \times 2)$-s superstructures. No obviously ordered structures were observed for SAMs prepared in hexane. The conditions under which OT molecules bound to the Au(111) surfaces depended on the solvent properties and determined whether the OT-SAMs included ordered or disordered phases. The intensity of the XPS S2 peak (161 eV) increased with increasing molecular randomness, which may be due to changes in the adsorption configurations of the OT molecules.

AUTHOR INFORMATION

Corresponding Author

*Ph +82-63-270-3410; Fax +82-63-270-3408; e-mail jrhahn@jbnu.ac.kr.

Notes

The authors declare no competing financial interest.

ACKNOWLEDGMENTS

This work was supported by grants from the Korean government (NRF) (2010-0024254 and 2007-0056333).

REFERENCES

(1) Ulman, A. *Chem. Rev.* **1996**, *96*, 1533−1554.
(2) Poirier, G. E. *Chem. Rev.* **1997**, *97*, 1117−1127.
(3) Seo, S.; Lee, H. *J. Phys. Chem. C* **2011**, *115*, 15480−15486.
(4) Azzam, W.; Bashir, A.; Terfort, A.; Strunskus, T.; Wöll, C. *Langmuir* **2006**, *22*, 3647−3655.
(5) Cyganik, P.; Buck, M. *J. Am. Chem. Soc.* **2004**, *126*, 5960−5961.
(6) Azzam, W.; Cyganik, P.; Witte, G.; Buck, M.; Wöll, C. *Langmuir* **2003**, *19*, 8262−8270.
(7) Yamada, R.; Wano, H.; Uosaki, K. *Langmuir* **2000**, *16*, 5523−5525.
(8) Love, J. C.; Estroff, L. A.; Kriebel, J. K.; Nuzzo, R. G.; Whitesides, G. M. *Chem. Rev.* **2005**, *105*, 1103−1169.
(9) Vericat, C.; Vela, M. E.; Benitez, G. A.; Gago, J. A. M.; Torrelles, X.; Salvarezza, R. C. *J. Phys.: Condens. Matter* **2006**, *18*, R867−R900.
(10) Schreiber, F. *Prog. Surf. Sci.* **2000**, *65*, 151−257.
(11) Poirier, G. E.; Pylant, E. D. *Science* **1996**, *272*, 1145−1148.
(12) Dishner, M. H.; Hemminger, J. C.; Feher, F. J. *Langmuir* **1997**, *13*, 2318−2322.
(13) Poirier, G. E. *Langmuir* **1997**, *13*, 2019−2026.
(14) Rohwerder, M.; de Weldige, K.; Stratmann, M. *J. Solid State Electrochem.* **1998**, *2*, 88−93.
(15) Torrelles, X.; Barrena, E.; Munuera, C.; Rius, J.; Ferrer, S.; Ocal, C. *Langmuir* **2004**, *20*, 9396−9402.
(16) Fenter, P.; Eisenberger, P.; Liang, K. S. *Phys. Rev. Lett.* **1993**, *70*, 2447−2450.
(17) Touzov, I.; Gorman, C. B. *J. Phys. Chem. B* **1997**, *101*, 5263−5276.
(18) Paradis, E.; Rowntree, P. *J. Electroanal. Chem.* **2003**, *550*, 175−185.
(19) Nuzzo, R. G.; Korenic, E. M.; Dubois, L. H. *J. Chem. Phys.* **1990**, *93*, 767−773.
(20) Muller-Meskamp, L.; Lussem, B.; Karthauser, S.; Waser, R. *J. Phys. Chem. B* **2005**, *109*, 11424−11426.
(21) Riposan, A.; Liu, G.-Y. *J. Phys. Chem. B* **2006**, *110*, 23926−23937.
(22) Zhang, J.; Chi, Q.; Ulstrup, J. *Langmuir* **2006**, *22*, 6203−6213.
(23) Poirier, G. E.; Tarlov, M. J. *Langmuir* **1994**, *10*, 2853−2856.
(24) Anselmetti, D.; Baratoff, A.; Guntherodt, H. J.; Gerber, C.; Michel, B.; Rohrer, H. *Europhys. Lett.* **1994**, *27*, 365−370.
(25) Lüssem, B.; Müller-Meskamp, L.; Karthäuser, S.; Waser, R. A. *Langmuir* **2005**, *21*, 5256−5258.
(26) Zeng, C. G.; Li, B.; Wang, B.; Wang, H. Q.; Wang, K. D.; Yang, J. L.; Hou, J. G.; Zhu, Q. S. *J. Chem. Phys.* **2002**, *117*, 851−856.
(27) Noh, J.; Hara, M. *Langmuir* **2002**, *18*, 1953−1956.
(28) Noh, J.; Kato, H. S.; Kawai, M.; Hara, M. *J. Phys. Chem. B* **2006**, *110*, 2793−2797.
(29) Mamun, A. H. A.; Hahn, J. R. *Surf. Sci.* **2012**, *606*, 664−669.
(30) Bain, C. D.; Troughton, E. B.; Tao, Y.-T.; Evall, J.; Whitesides, G. M.; Nuzzo, R. G. *J. Am. Chem. Soc.* **1989**, *111*, 321−335.
(31) Peterlinz, K. A.; Georgiadis, R. *Langmuir* **1996**, *12*, 4731−4740.
(32) Dannenberger, O.; Wolff, J. J.; Buck, M. *Langmuir* **1998**, *14*, 4679−4682.
(33) Lee, N.-S.; Kang, H.; Ito, E.; Hara, M.; Noh, J. *Bull. Korean Chem. Soc.* **2010**, *31*, 2137−2138.
(34) Kim, M.; Hohman, J. N.; Serino, A. C.; Weiss, P. S. *J. Phys. Chem. C* **2010**, *114*, 19744−19751.
(35) Kudelski, A.; Hill, W. *Langmuir* **1999**, *15*, 3162−3168.
(36) Yamada, R.; Sakai, H.; Uosaki, K. *Chem. Lett.* **1999**, *7*, 667−668.
(37) Kim, D. H.; Noh, J.; Hara, M.; Lee, H. *Bull. Korean Chem. Soc.* **2001**, *22*, 276−280.
(38) Umemura, K.; Fujita, K.; Ishida, T.; Hara, M.; Sasabe, H.; Knoll, W. *Jpn. J. Appl. Phys.* **1998**, *37*, 3620−3625.
(39) Noh, J.; Konno, K.; Ito, E.; Hara, M. *Jpn. J. Appl. Phys.* **2005**, *44*, 1052−1054.
(40) Jeong, Y.; Chung, H.; Noh, J. *Colloids Surf., A* **2008**, *313*, 608−611.
(41) Camillone, N., III; Eisenberger, P.; Leung, T. Y. B.; Schwartz, P.; Scoles, G.; Poirier, G. E.; Tarlov, M. J. *J. Chem. Phys.* **1994**, *101*, 11031−11036.
(42) Delamarche, E.; Michel, B. *Thin Solid Films* **1996**, *273*, 54−60.
(43) Schönenberger, C.; Jorritsma, J.; Sondag-Huethorst, J. A. M.; Fokkink, L. G. J. *J. Phys. Chem.* **1995**, *99*, 3259−3271.
(44) Delamarche, E.; Michel, B.; Kang, H.; Gerber, Ch. *Langmuir* **1994**, *10*, 4103−4108.
(45) McCarley, R. L.; Dunaway, D. J.; Willicut, R. J. *Langmuir* **1993**, *9*, 2775−2777.
(46) Bucher, J.-P.; Santesson, L.; Kern, K. *Langmuir* **1994**, *10*, 979−983.

(47) Bumm, L. A.; Arnold, J. J.; Charles, L. F.; Dunbar, T. D.; Allara, L. D.; Weiss, P. S. *J. Am. Chem. Soc.* **1999**, *121*, 8017−8021.
(48) Xiao, X.; Wang, B.; Zhang, C.; Yang, Z.; Loy, M. M. T. *Surf. Sci.* **2001**, *472*, 41−50.
(49) Donhauser, Z. J.; Price, D. W.; Tour, J. M.; Weiss, P. S. *J. Am. Chem. Soc.* **2003**, *125*, 11462−11463.
(50) Poirier, G. E.; Tarlov, M. J. *J. Phys. Chem.* **1995**, *99*, 10966−10970.
(51) Cavalleri, O.; Hirstein, A.; Kern, K. *Surf. Sci.* **1995**, *340*, L960−L964.
(52) Mamun, A. H. A; Son, S. B.; Hahn, J. R. *Bull. Korean Chem. Soc.* **2011**, *32*, 281−285.
(53) Yang., G.; Liu, G.-Y. *J. Phys. Chem. B* **2003**, *107*, 8746−8759.
(54) Yan, D.; Saunders, J. A.; Jennings, G. K. *Langmuir* **2000**, *16*, 7562−7565.
(55) Li, F.; Tang, L.; Zhou, W.; Guo, Q. *J. Am. Chem. Soc.* **2010**, *132*, 13059−13063.
(56) Dubois, L. H.; Zegarswki, R.; Nuzzo, R. G. *J. Chem. Phys.* **1993**, *98*, 678−688.
(57) Camillone, N., III; Leung, T. Y. B.; Schwartz, P.; Eissenberger, P.; Scoles, G. *Langmuir* **1996**, *12*, 2737−2746.
(58) Poirier, G. E.; Tarlov, M. J.; Rushmeirer, H. E. *Langmuir* **1994**, *10*, 3383−3386.
(59) Poirier, G. E. *Langmuir* **1999**, *15*, 1167−1175.
(60) Voets, J.; Gerritsen, J. W.; Grimbergen, R. F. P.; Van Kempen, H. *Surf. Sci.* **1998**, *399*, 316−323.
(61) Staub, R.; Toerker, M.; Fritz, T.; Schmitz-Hűbsch, T.; Sellam, F.; Leo, K. *Langmuir* **1998**, *14*, 6693−6698.
(62) Dai, J.; Li, Z.; Jin, J.; Cheng, J.; Kong, J.; Bi, S. *J. Electroanal. Chem.* **2008**, *624*, 315−322.
(63) Kondoh, H.; Iwasaki, M.; Shimada, T.; Amemiya, K.; Yokohama, T.; Ohta, T.; Shimomura, M.; Kono, S. *Phys. Rev. Lett.* **2003**, *90*, 66102−1−66102−4.
(64) Fenter, P.; Schreiber, F.; Berman, L.; Scoles, G.; Eisenberger, P.; Bedzyka, M. J. *Surf. Sci.* **1998**, *412/413*, 213−235.
(65) Dubois, L. H.; Nuzzo, R. G. *Annu. Rev. Phys. Chem.* **1992**, *43*, 437−463.
(66) Ulman, A.; Eilers, J. E.; Tillman, N. *Langmuir* **1989**, *5*, 1147−1152.
(67) Teràn Arce, F.; Vela, M. E.; Salvarezza, R. C.; Arvia, A. J. *J. Chem. Phys.* **1998**, *109*, 5703−5706.
(68) Fenter, P.; Eberhardt, A.; Eisenberger, P. *Science* **1994**, *266*, 1216−1218.
(69) Ulman, A. *An Introduction to Ultrathin Organic Films: From Langmuir-Blodgett to Self-Assembly*; Academic Press: Boston, 1991.
(70) Heister, K.; Zharnikov, M.; Grunze, M.; Johansson, L. S. O.; Ulman, A. *Langmuir* **2001**, *17*, 8−11.
(71) Kluth, G. J.; Carro, C.; Maboudian, R. *Phys. Rev. B* **1999**, *59*, R10449−R10452.
(72) Roper, M. G.; Shegg, M. P.; Fisher, C. J.; Lee, J. J.; Dhanak, V. R.; Woodruff, D. P.; Jones, R. G. *Chem. Phys. Lett.* **2004**, *389*, 87−91.
(73) Vargas, M. C.; Giannozzi, P.; Selloni, A.; Scoles, G. *J. Phys. Chem. B* **2001**, *105*, 9509−9513.
(74) Beardmore, K. M.; Kress, J. D.; Bishop, A. R.; Gronbech-Jensen, N. *Synth. Met.* **1997**, *84*, 317−318.
(75) Hayashi, T.; Morikawa, Y.; Nozoye, H. *J. Chem. Phys.* **2001**, *114*, 7615−7621.
(76) Teràn Arce, F.; Vela, M. E.; Salvarezza, R. C.; Arvia, A. J. *Langmuir* **1998**, *14*, 7203−7212.
(77) Castner, D. G.; Hinds, K.; Grainger, D. W. *Langmuir* **1996**, *12*, 5083−5086.
(78) Ishida, T.; Hara, M.; Kojima, M.; Tsuneda, S.; Nishida, N.; Sasabe, H.; Knoll, W. *Langmuir* **1998**, *14*, 2092−2096.
(79) Ishida, T.; Choi, N.; Mizutani, W.; Tokumoto, H.; Kojima, I.; Azehara, H.; Hokari, H.; Akiba, U.; Fujihira, M. *Langmuir* **1999**, *15*, 6799−6806.
(80) Buckel, F.; Effenberger, F.; Yan, C.; Gölzhäuser, A.; Grunze, M. *Adv. Mater.* **2000**, *12*, 901−905.
(81) Zhong, C.-J.; Brush, R. C.; Anderegg, J.; Poter, M. D. *Langmuir* **1999**, *15*, 518−525.
(82) Wirde, M.; Gelius, U.; Nyholm, L. *Langmuir* **1999**, *15*, 6370−6378.
(83) Jeong, Y.; Lee, C.; Ito, E.; Hara, M.; Noh, J. *Jpn. J. Appl. Phys.* **2006**, *45*, 5906−5910.
(84) Leavitt, A. J.; Beebe, T. P. *Surf. Sci.* **1994**, *314*, 23−33.
(85) Yamada, R.; Uosaki, K. *Langmuir* **1997**, *13*, 5218−5221.
(86) Yamada, R.; Uosaki, K. *Langmuir* **1998**, *14*, 855−861.
(87) Dannenberger, O.; Wolff, J. J.; Buck, M. *Langmuir* **1998**, *14*, 4679−4682.
(88) Reichardt, C. *Chem. Rev.* **1994**, *94*, 2319−2358.
(89) Barton, A. F. M. *Chem. Rev.* **1975**, *75*, 731−753.
(90) Yan, D.; Saunders, J. A.; Jennings, G. K. *Langmuir* **2002**, *18*, 10202−10212.
(91) Yan, D.; Saunders, J. A.; Jennings, G. K. *Langmuir* **2003**, *19*, 9290−9296.
(92) Bensebaa, F.; Voicu, R.; Huron, L.; Ellis, T. H.; Kruus, E. *Langmuir* **1997**, *13*, 5335−5340.
(93) Laffineur, F.; Couturier, N.; Delhalle, J.; Mekhalif, Z. *Appl. Surf. Sci.* **2003**, *212*, 452−457.
(94) Mekhalif, Z.; Laffineur, F.; Couturier, N.; Delhalle, J. *Langmuir* **2003**, *19*, 637−645.
(95) Sur, U. K.; Lakshminarayanan, V. *J. Electroanal. Chem.* **2001**, *516*, 31−38.
(96) Finklea, H. O.; Avery, S.; Lynch, M.; Furtsch, T. *Langmuir* **1987**, *3*, 409−413.